Complexes of Horseradish Peroxidase with Formate, Acetate, and Carbon Monoxide †

ARTICLE *in* BIOCHEMISTRY · FEBRUARY 2005

Impact Factor: 3.02 · DOI: 10.1021/bi0483211 · Source: PubMed

5 AUTHORS, INCLUDING:

Gunilla H Carlsson
Uppsala University
8 PUBLICATIONS **541** CITATIONS
SEE PROFILE

Peter Nicholls
University of Essex
213 PUBLICATIONS **4,695** CITATIONS
SEE PROFILE

Dimitri A Svistunenko
University of Essex
88 PUBLICATIONS **3,066** CITATIONS
SEE PROFILE

Complexes of Horseradish Peroxidase with Formate, Acetate, and Carbon Monoxide†

Gunilla H. Carlsson,‡ Peter Nicholls,§ Dimitri Svistunenko,§ Gunnar I. Berglund,‡ and Janos Hajdu*,‡

Molecular Biophysics, Institute of Cellular and Molecular Biology, Uppsala University, Husargatan 3 (Box 596), SE-75124 Uppsala, Sweden, and Department of Biological Sciences, University of Essex, Wivenhoe Park, Colchester, Essex CO4 3SQ, U.K.

Received August 5, 2004; Revised Manuscript Received October 21, 2004

ABSTRACT: Carbon monoxide, formate, and acetate interact with horseradish peroxidase (HRP) by binding to subsites within the active site. These ligands also bind to catalases, but their interactions are different in the two types of enzymes. Formate (notionally the "hydrated" form of carbon monoxide) is oxidized to carbon dioxide by compound I in catalase, while no such reaction is reported to occur in HRP, and the CO complex of ferrocatalase can only be obtained indirectly. Here we describe high-resolution crystal structures for HRP in its complexes with carbon monoxide and with formate, and compare these with the previously determined HRP−acetate structure [Berglund, G. I., et al. (2002) *Nature 417*, 463−468]. A multicrystal X-ray data collection strategy preserved the correct oxidation state of the iron during the experiments. Absorption spectra of the crystals and electron paramagnetic resonance data for the acetate and formate complexes in solution correlate electronic states with the structural results. Formate in ferric HRP and CO in ferrous HRP bind directly to the heme iron with iron−ligand distances of 2.3 and 1.8 Å, respectively. CO does not bind to the ferric iron in the crystal. Acetate bound to ferric HRP stacks parallel with the heme plane with its carboxylate group 3.6 Å from the heme iron, and without an intervening solvent molecule between the iron and acetate. The positions of the oxygen atoms in the bound ligands outline a potential access route for hydrogen peroxide to the iron. We propose that interactions in this channel ensure deprotonation of the proximal oxygen before binding to the heme iron.

Heme enzymes have a pivotal role in biology. The chemical diversity of these proteins is striking, yet the biological oxidation reactions they catalyze involve similar high-oxidation state intermediates whose reactivities are modulated by the protein environment. Figure 1 shows the key redox reactions promoted by horseradish peroxidase (HRP).[1] The main overall reaction catalyzed by peroxidases can be summarized as $H_2O_2 + 2AH \rightarrow 2H_2O + 2A^*$, where AH represents a reducing substrate and A* is a free radical product. This reaction involves several steps with two highly oxidized heme intermediates, compound I and compound II (Figure 1). HRP can also convert hydrogen peroxide to water and dioxygen ($2H_2O_2 \rightarrow 2H_2O + O_2$). This is the "catalatic" or catalase-like activity of the enzyme (*1*−*4*), but in contrast to true catalases, the rate of this reaction in HRP is slow.

HRP activity is influenced by small molecule ligands, including carbon monoxide, cyanide, azide, and fluoride, as well as formate and acetate (for reviews, see refs *5* and *6*). Both acetate and formate bind to ferric horseradish peroxidase (*7*), formate more strongly than acetate. No EPR studies have apparently been carried out previously with the carboxylic acids. Early EPR and magnetic susceptibility studies

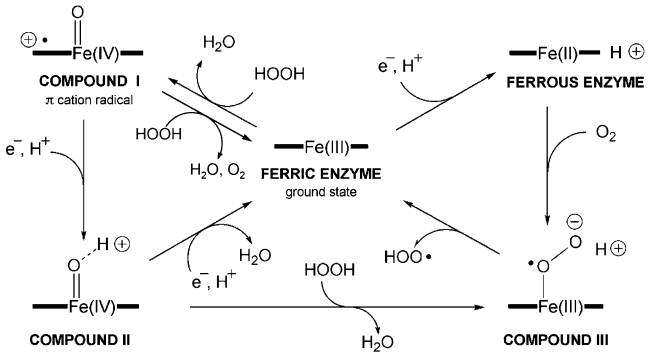

FIGURE 1: Reactions catalyzed by horseradish peroxidase.

suggested that unliganded ferric HRP at neutral pH exists in a mixture of spin states (*8*, *9*). Addition of a ferric ligand such as cyanide or fluoride secures 100% occupancy of a unique low-spin (cyanide) or high-spin (fluoride) state. A well-defined high-spin state with moderate rhombicity of the $g = 6$ electron paramagnetic resonance (EPR) signal can also be achieved by benzhydroxamate. Benzhydroxamate binds in the heme pocket, but it does not interact directly with the heme iron of HRP (*10*, *11*). Binding of the classical high-spin (fluoride or formate) and the low- or mixed-spin (cyanide or azide) ligands involves uptake of anion and proton or free acid (*12*−*14*). Binding of such ligands is mutually exclusive and fully competitive toward peroxide binding. In contrast, nitrate, acetate, and perchlorate bind as anions alone but to an acid form of the enzyme (*15*, *16*), and these ligands are only partially competitive toward

† This work was supported by the Swedish Research Councils.

* To whom correspondence should be addressed. E-mail: janos@xray.bmc.uu.se. Telephone: 46-18-4714449. Fax: 46-18-511755.

‡ Uppsala University.

§ University of Essex.

[1] Abbreviations: EPR, electron paramagnetic resonance; HP, *Helicobacter pylori*; HRP, horseradish peroxidase; PEG, polyethylene glycol; PM, *Proteus mirabilis*.

10.1021/bi0483211 CCC: $30.25
Published on Web 12/18/2004

Table 1: Data Collection and Refinement Statistics for HRP in Complex with Acetate (*17*), Formate, and Carbon Monoxide

	acetate in ferric HRP	formate in ferric HRP	CO in ferrous HRP
Figure, PDB entry	4A, 1H5A	4B, 1W4W	4C, 1W4Y
no. of crystals used	7	7	1
degrees per crystal	15	15	100
X-ray wavelength (Å)	0.931	1.089	1.089
$P2_12_12_1$ cell [*a*, *b*, *c* (Å)]	40.3, 67.8, 117.3	40.3, 68.3, 117.0	40.4, 67.6, 117.2
resolution range (Å)	19.7−1.60	26.8−1.52	25.9−1.57
outer shell (Å)	1.64−1.60	1.57−1.52	1.61−1.57
total no. of reflections	183656	581986	558551
no. of unique reflections	42167	49541	41633
completeness (%)	97.7 (93.9)	96.0 (78.7)	90.4 (86.8)
$\langle I/\sigma(I)\rangle$	18.2	12.1	8.3
R_{merge} (%)[a]	5.8 (20.3)	6.8 (24.3)	7.0 (30.1)
refinement			
highest resolution used (Å)	1.60	1.55	1.60
completeness (%)	97.7 (93.9)	97.8 (94.9)	90.6
no. of atoms	2906	2802	2764
no. of waters	404	354	341
average *B* factor (Å^2)			
all	16.7	14.8	16.3
water	27.2	23.0	23.3
not water	15.0	13.7	15.3
R_{cryst} (%)[b]	17.8	19.8	19.9
R_{free} (%)[c]	20.2	21.5	21.1

[a] $R_{merge} = \sum|I - I_{average}|/\sum I$, where I is the observed intensity of a reflection and $I_{average}$ is the average intensity obtained from multiple observations of symmetry-related reflections. [b] $R_{cryst} = \sum||F_{obs}| - |F_{calc}||/\sum|F_{obs}|$. [c] Five percent of the data were excluded from refinement and used to calculate R_{free} (*60*).

peroxides or the classical ligands. Their interaction thus differs from that of the classical high-spin ligands such as chloride, fluoride, and formate. These differences suggested that formate binding will differ from acetate binding. While the structure of HRP in complex with acetate was determined previously (*17*), no structure has been reported of a plant peroxidase in complex with formate.

Very recently, structures have been published for two catalases in complex with formate [catalase from *Proteus mirabilis* to 2.3 Å resolution, Protein Data Bank (PDB) entry 1nm0 (*18*) and catalase from *Helicobacter pylori* to 1.6 Å resolution, PDB entry 1qwm (*19*)]. Unlike peroxidases, catalase compound I is reduced to ferric catalase by formate but not acetate (*20*−*22*). This reduction of compound I has been suggested to be physiologically relevant (*23*). In catalase, both formate and acetate react with the ferric heme iron to form similar high-spin complexes. Formate also reacts with catalase peroxide compound II to form an unstable complex which decays in a one-electron process to give free ferric catalase formate (*24*, *25*). The apparent affinity for formate and compound II is either close to [horse liver catalase (*24*)] or ∼10 times lower than [beef liver catalase (*25*)] the corresponding affinity for formate and unliganded ferric catalase.

HRP can be reduced to its ferrous form with dithionite and then reacts with CO (*1*, *26*). The resulting CO complex is spectrally similar to that formed by myoglobin and hemoglobin, although detailed analysis suggests a more complicated structure (*27*). The dissociation of CO from the HRP−CO complex is very slow, indicating a structural stabilization not available to other hemoprotein−CO complexes (*28*). CO binding was found to involve a proton, and Hayashi et al. (*29*) proposed that the bound CO is stabilized by a hydrogen bond to a distal residue. In several respects, therefore, the HRP−CO complex is expected to differ from the classical hemoglobin and myoglobin complexes.

This paper describes high-resolution crystal structures of HRP in complex with carbon monoxide and formate, and compares these structures with the previously determined structures of the acetate−HRP complex and unliganded ferrous HRP (*17*). We also present EPR and UV−visible spectroscopic data for the acetate− and formate−peroxidase complexes in solution, and discuss the mechanistic implications of our findings.

MATERIALS AND METHODS

Crystal Preparation. Recombinant HRP isoenzyme C (*30*) was a gift of A. T. Smith (University of Sussex, Brighton, U.K.). The enzyme was crystallized at 4 °C from 20% polyethylene glycol (PEG) 8000, 0.2 M calcium acetate, and 0.1 M sodium cacodylate (pH 6.5) with ferulic acid as an additive (*31*). Large single crystals were obtained by streak seeding in hanging drops.

Preparation of the Formate Complex. Crystals of ferric HRP were transferred to 10 μL droplets of 20% PEG 8000, 0.2 M magnesium formate, and 0.1 M sodium cacodylate (pH 6.5) and left for more than 3 h at 8 °C before being frozen in liquid nitrogen.

Preparation of the Ferrous−Carbon Monoxide Complex. Crystals of ferric HRP were transferred to 10 μL droplets of 20% PEG 8000, 10% PEG 300, 0.2 M calcium acetate, and 0.1 M sodium cacodylate (pH 6.5). The ferric crystals were moved into a glovebox under a nitrogen atmosphere and left to equilibrate overnight. One microliter of 100 mM sodium dithionite was then added to the droplet, and after at least 1 h in this reducing solution, a crystal was placed into a cryoloop and exposed to carbon monoxide at a pressure of 10 bar for 10 min in a pressure cell (4DX-ray Systems AB, www.4dx.se). The pressure cell was then moved out of the glovebox and the crystal rapidly frozen in liquid nitrogen. The absorbance spectrum of the crystal at 100 K was consistent with a carbon monoxide−ferrous HRP complex.

However, the same procedure did not produce measurable spectral changes in crystals of ferric HRP.

X-ray diffraction data were collected at beamline 711 of MaxLab (Lund, Sweden) at temperatures between 90 and 100 K, and at a wavelength of 1.089 Å. In the case of ferric crystals, we used a multicrystal data collection strategy (*17*) to minimize the radiation-induced reduction of the iron center. The oxidation state of the crystals was monitored by a single-crystal microspectrophotometer (4DX-ray Systems AB, www.4dx.se) (*32*). Fifteen degrees of data were collected systematically from each of seven crystals to give a composite data set (*17*), corresponding to a total of 90° of rotation. No such measures were necessary with the ferrous HRP−CO complex, where 100° of data could be collected from a single crystal without measurable changes in its UV−visible absorption spectrum. Data were processed and scaled using the HKL package (*33*) and programs in the CCP4 suite (*34*). Initial rounds of refinement were carried out in CNS (*35*) based on PDB entry 1H5A for formate and PDB entry 1H58 for CO without waters, calcium, or acetate in the starting model. In the last rounds of refinement, rebuilding was carried out in maps calculated using ARP/wARP version 5.0 (*36*−*39*), and as a last step, the position of the ligand was refined as a rigid body using only X-ray terms. Crystallographic statistics are listed in Table 1.

UV−Visible Spectrophotometry (Solution Studies). UV−visible spectra were obtained with a Cary 5 spectrophotometer at 25 °C, and data were analyzed with MS Excel. Conditions are described in the legend of Figure 2.

Electron Paramagnetic Resonance Spectroscopy. EPR data were obtained at 10 K on a Bruker EMX EPR spectrometer equipped with an Oxford Instruments liquid helium system, and a spherical high-quality Bruker resonator (SP9703). Samples (0.25 mL) were frozen in Wilmad EPR tubes in a methanol/dry ice slurry, and then transferred into a liquid nitrogen storage container prior to measurements at 10 K. The samples in Figure 3 contained 88 μM HRP (heme), 0.1 M potassium phosphate buffer (pH 6.0), and 0.4 M potassium acetate or 0.2 M sodium formate. Horseradish peroxidase used for EPR and UV−visible studies was Biozyme HRP 4C, which is predominantly isoenzyme C (the isoenzyme used for structural studies). Comparisons showed no significant differences between the crystal and the commercial samples.

RESULTS

Figure 2A shows the UV−visible spectra of free HRP, acetate-bound HRP, and formate-bound HRP. As with other weak acid ligands, the binding becomes stronger as the pH decreases. At room temperature, formate binds with a K_d of ≈30 mM at pH 5.1 while the corresponding K_d for acetate is in excess of 300 mM. The formate species is spectroscopically similar to formate−catalase and formate−metmyoglobin complexes, with a sharpening and increase in intensity of the Soret band, with the removal of the shoulder on this peak seen in the unliganded enzyme, and a modest blue shift of the charge transfer bands in the visible region. The acetate-induced spectral change, unlike that seen with catalase and metmyoglobin, involves an increased asymmetry of the Soret peak and a small but distinct red shift of the charge transfer band above 600 nm (see Figure 2B for the difference

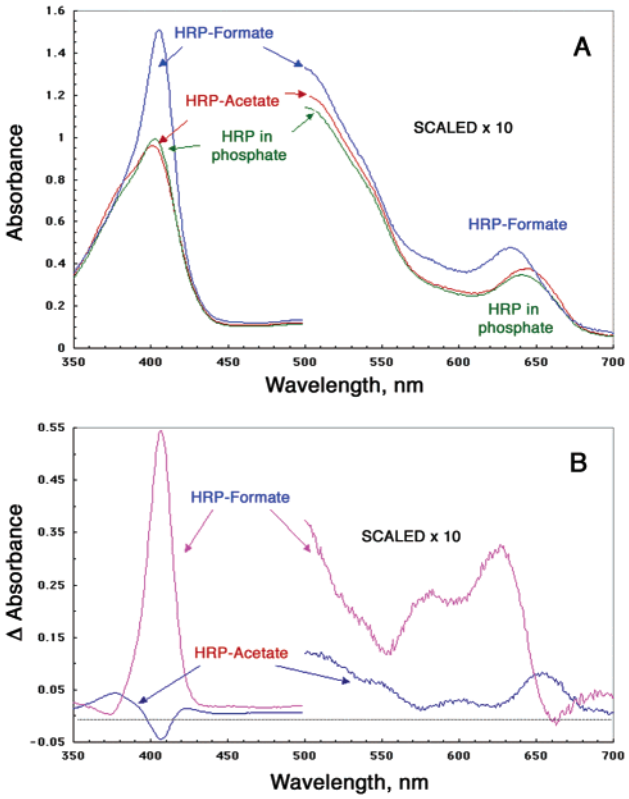

FIGURE 2: UV−visible spectra of HRP and its complexes with acetate and formate. (A) Absolute spectra are for the native enzyme, the HRP−formate complex, and the HRP−acetate complex (spectra in the visible region on the right are plotted on a 10-fold expanded scale). (B) Difference spectra are for the formate and acetate complexes minus the spectrum of the unliganded native enzyme. Conditions: 11.5 μM HRP in 0.05 M potassium phosphate (pH 6.0), with or without 0.7 M sodium formate, 11.5 μM HRP in 0.8 M sodium acetate (pH 5.0), 25 °C, Cary 5 spectrophotometer, 0.75 mL sample volumes, 1 cm path length, semimicro cuvettes.

spectra). These differences are consistent with the findings of Araiso and Dunford (*15*, *16*) with formate binding in a conventional high-spin manner analogous to the paradigm high-spin ligand fluoride but acetate binding in an alternative manner only partially competitive with Fe-coordinating ligands and peroxides.

Electronic differences between the formate and acetate complexes are confirmed by the EPR data shown in Figure 3. The key differences are between more axial and more rhombic high-spin signals in the $g = 6$ region of the spectrum. As reported previously, the unliganded enzyme is a mixture of at least two species with different rhombicities. Acetate and formate both simplify the spectra, creating essentially a single electronic species with acetate forming a species with wide separation of the $g = 6$ components and formate producing a species with a much narrower separation of the two $g = 6$ components.

Figure 4 shows the structures of acetate (*17*), formate, and carbon monoxide bound to the active site of HRP at resolutions of 1.60, 1.55, and 1.60 Å, respectively (see also Table 1). Acetate (Figure 4A) stacks parallel with the heme plane, and both of its oxygens form hydrogen bonds with Arg38. In addition, one of the oxygens also binds to His42. The other oxygen takes up a position above the heme iron, but it is too far from it (3.6 Å) for direct interaction. There is no space for an intervening solvent molecule between the

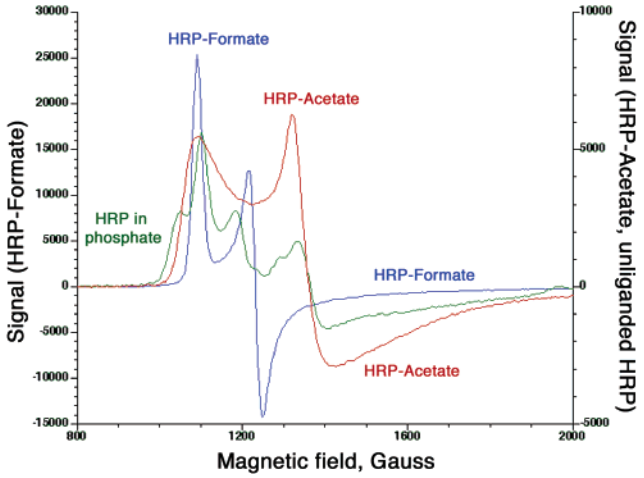

FIGURE 3: Key features of the high-spin $g = 6$ region of the EPR spectra of HRP and its acetate and formate complexes [88 μM HRP in 0.1 M potassium phosphate (pH 6.0), either alone or with 150 mM sodium formate or 300 mM sodium acetate, as indicated]. Samples (0.5 mL) were prepared at room temperature, and 0.25 mL aliquots were frozen as described in Materials and Methods. EPR spectra were then obtained at 10 K. The formate−HRP spectrum is plotted using the left-hand *Y*-axis (arbitrary units); the acetate−HRP and native enzyme spectra are plotted using the expanded right-hand *Y*-axis. Instrumental conditions were as follows: microwave power of 3.2 mW, microwave frequency of 9.467 GHz, modulation amplitude of 5 G, spectrum scan rate of 35.7 G/s, time constant of 82 ms, single scan.

iron and the carboxylate of acetate. This explains the observed spectral features in Figures 2 and 3 for this complex.

Formate (Figure 4B) binds directly through one of its oxygens to the iron (O−Fe distance of 2.3 Å), and this is clearly indicated by the spectral changes. The carboxylate of formate is rotated by ~90° relative to the carboxylate of acetate, and both oxygens of formate interact with Arg38. The distal oxygen of formate also forms a strong hydrogen bond with His42. The positions of formate and acetate overlap through this distal oxygen atom (hydrogen-bonded to Arg38 and His42 in both structures). We note that acetate (Figure 4A) cannot bind to the iron in the same way as formate (Figure 4B) because its methyl group clashes with the heme plane when its carboxylate is rotated into the position of formate. This suggests that the difference in the behavior of these two ligands in HRP is primarily due to steric factors. No other binding site could be observed for formate in the crystal, while a puzzling 36 binding sites have been reported for formate within the crystallographic asymmetric unit of the *H. pylori* catalase (*19*).

Table 2: Iron−Ligand Distances in High-Resolution X-ray Structures of Carbon Monoxide Bound to Heme Proteins

ferrous hemoprotein	PDB entry	resolution (Å)	Fe−C distance (Å)	Fe−C−O angle (deg)
nitric oxide reductase cytochrome P450nor (*61*)	1JFC	1.05	1.8	172
sperm whale myoglobin (*62*)	1A6G	1.15	1.8	171
sperm whale myoglobin (*63*)	1BZR	1.15	1.7	171
sperm whale myoglobin	1JW8	1.30	1.8	176
horse heart myoglobin (*64*)	1DWR	1.45	1.9	162
human hemoglobin β-subunit (*65*)	1J40	1.45	1.6−1.7	168−175
cytochrome cd_1 nitrite reductase (*66*)	1DY7	1.60	1.9	158
HRP (this work)	1W4Y	1.60	1.8	171

Carbon monoxide (Figure 4C) binds more or less perpendicularly to the heme plane with an Fe−C−O angle of 171° and an iron−carbon distance of 1.8 Å. No other densities indicating secondary CO binding are seen close to the heme group. The angles and distances between the oxygen atom of CO and the side chains of His42 and Arg38 indicate two hydrogen bonds between the protein and the bound CO molecule: a strong hydrogen bond with His42 and a weaker one with Arg38. These interactions stabilize the bound CO, leading to a lower than usual dissociation constant of CO in the ferrous HRP−CO complex (*28*). These findings are also in agreement with the proposal of Hayashi et al. (*29*) about the involvement of a proton in CO binding. In stereochemical terms, the geometry of CO binding is very similar to the binding geometries of CO in other heme proteins; the Fe−C−O angle = 158−174°, and the Fe−C distance = 1.7−2.1 Å (Table 2). The Fe−C−O angle is in fact closer to 180° than in carboxymyoglobin and in some carboxyhemoglobin structures.

DISCUSSION

The active site of HRP represents an adaptive environment for ligand binding. Several hydrogen bonding possibilities are available with both Arg38 and His42, and the different interactions could be utilized at different stages of catalysis. The positions of the oxygen atoms of the ligands in Figure 4 outline a potential access route for hydrogen peroxide to the iron. Interactions with residues in this channel could

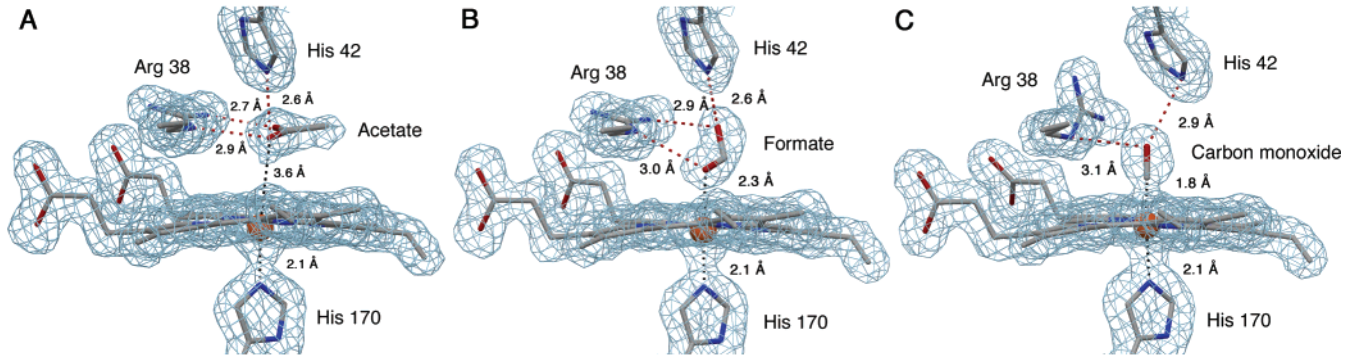

FIGURE 4: Refined crystal structures, showing the active site of horseradish peroxidase in complex with acetate (A), formate (B), and carbon monoxide (C). Shown are SigmaA-weighted $2mF_o - DF_c$ electron density maps (*55*) contoured at 1σ, where σ represents the root-mean-square electron density for the unit cell. The overall coordinate error is 0.2 Å in the structures. This figure was prepared with Molscript (*56*−*59*) and The Gimp (www.gimp.org).

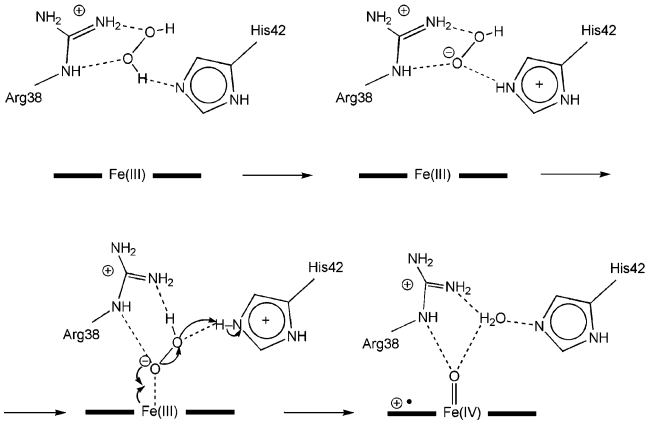

FIGURE 5: Proposed mechanism for the formation of compound I in HRP.

secure deprotonation of the proximal oxygen (Figure 5). There are currently no direct structural data to show how hydrogen peroxide binds at the active site. Studies on the R38L mutant of HRP (*40*) and on polyethylene glycolated HRP in organic solvent (*41*) suggest the involvement of a hydrogen peroxide complex in the catalytic cycle, and experiments at cryogenic temperatures identified a peroxoanion−iron III complex, compound 0, as a compound I precursor (*42*−*44*).

Formation of HRP Compound I. Using the structures of compounds I and III (*17*) together with those of the acetate and formate complexes (from this work), a mechanism for hydrogen peroxide binding and compound I formation may be proposed (Figure 5). Our results show that the channel, providing access to the heme iron, involves sites where acetate and formate bind. Hydrogen peroxide can readily be accommodated in either site for formation of hydrogen bonds with Arg38 and His42. During catalysis, a proton must be removed from hydrogen peroxide and transferred to another group in the active site. A number of authors (*17*, *28*, *29*, *45*) have suggested that this proton acceptor is His42, and this proposal is adopted in the model (Figure 5). In the HRP−acetate and HRP−formate complexes, His42 forms hydrogen bonds to the carboxylate oxygens of these ligands. If hydrogen peroxide initially binds at the position of the carboxylate group of acetate, then His42 would be ideally poised to accept a proton from the proximal peroxide oxygen. The hydroperoxo anion could be stabilized in this position by hydrogen bonds from Arg38 Nϵ and Arg38 Nη. In the next step, the hydroperoxo anion binds to the iron. Following transfer of a proton from His42 to the distal oxygen in the hydroperoxo−ferric heme complex, the O−O bond undergoes heterolytic cleavage to give water and compound I.

Formation of the Carbonmonoxy−HRP Complex in Light of the Structural Results. Infrared spectral data indicate two different binding modes for CO in ferrous HRP (*46* and references therein). The form with a lower stretching frequency (1905 cm^{-1}) is the main species at lower pH, but it disappears at high pH where a form with a frequency of 1933 cm^{-1} is present, with a transition p*K* of 8.8 (*47*). The 1932 cm^{-1} mode is believed to represent binding normal to the heme plane, while the other mode is tilted (*46*). At low pH, there appeared to be an equilibrium between the two forms that was dependent upon the CO concentration, and Evangelista-Kirkup et al. (*46*) speculated that there is "an additional weak binding CO site whose occupancy changes the conformation of the distal residues in a manner that favors the formation of an H bond from the protonated distal histidine to the Fe-bound CO."

Feis et al. (*48*) have prepared HRP His42Leu and Arg38Leu mutants and suggest that the two forms correspond to hydrogen bonding to either Arg38 or His42. In our experiment, the crystals were exposed to excess CO and the bound CO is binding almost normal to the heme plane. No other CO molecule was observed in the structure. The reported slow dissociation of CO (*28*) is in part explained by the possible existence of two hydrogen bonds between CO and either or both distal residues, His42 and Arg38 (Figure 4C). The p*K* of 8.25 identified by Hayashi et al. (*29*) is presumably that of His42, as suggested by Feis et al. (*48*). At a more alkaline pH, the bound CO may still be stabilized by a hydrogen bond to the distal Arg38. Mutation of the latter to leucine (Arg38Leu) increases the rate of re-formation of the CO complex after photodissocation (*49*). Hydrogen bond formation may thus decrease the rate of binding of CO to the heme Fe while stabilizing the resulting product.

The Catalase-like Reaction of HRP: Implications for the Reaction of Hydrogen Peroxide with Compound I. The binding of formate and acetate in HRP shows certain similarities to the binding of formate in the active site of catalase from *H. pylori* (HP) (*19*). HP catalase crystallizes with two molecules in the asymmetric unit, each exhibiting a different orientation of the formate adjacent to the heme. The formate in molecule A is bound in the same orientation as the formate in *P. mirabilis* (PM) catalase (*18*), interacting with the heme iron at a distance of 2.7 Å. This interaction is also similar to the interaction of formate with the iron in HRP. The formate in molecule B of HP catalase is 3 Å above the heme plane with the closest oxygen 3.9 Å from the iron. The orientation of the formate in molecule B is similar to the orientation of the carboxylate in the HRP−acetate complex. The two different conformations of formate seen in HP catalase share the position of one oxygen atom, which is hydrogen bonded to His56 (2.6 and 2.8 Å, respectively, in the two molecules of the asymmetric unit).

HRP has a slow catalase-like activity (*2*, *4*). In this catalatic reaction of the enzyme, a second hydrogen peroxide molecule reacts with compound I to form a water molecule and dioxygen. Labeling studies show that in heme catalases, the dioxygen comes from the second hydrogen peroxide (*50* and reference therein) while the water is formed from the ferryl oxygen by the transfer of two protons and two electrons. Modeling a hydrogen peroxide molecule after the distal formate binding mode in HP catalase (*19*) and comparing it with the structure of PM catalase compound I (*18*) show how two protons could be abstracted from hydrogen peroxide. In this model, the proximal oxygen atom of the incoming hydrogen peroxide molecule would be within hydrogen bonding distance of the ferryl oxygen, while the distal oxygen atom would be within hydrogen bonding distance of His54 and Asn127 (approximately 2.8 and 2.6 Å, respectively). The protons are positioned to be transferred to the ferryl oxygen and to His54, while two electrons are moved to the oxyferryl group from the peroxo anion, leading to the formation of a water molecule and a dioxygen molecule. A similar mechanism (Figure 6) may be possible in HRP, although the geometric arrangement of the requisite

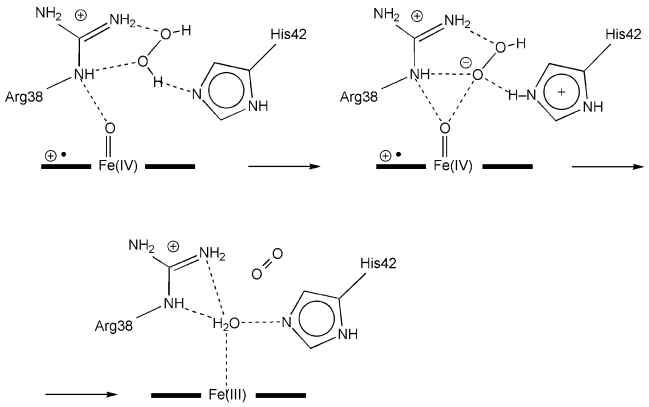

FIGURE 6: Possible mechanism for the reaction of compound I with hydrogen peroxide in the catalase-like reaction of HRP.

groups is not as favorable as in catalase. The catalase reaction of HRP is likely to be influenced by bound water molecules in the active site. It has been suggested by Jones (*51*) that the absence or presence of a water in the active site determines whether compound I reacts in a one-electron reduction process (which is the normal reaction for peroxidases) or in a two-electron reaction (as catalases do). In the compound I form of HRP, a water molecule forms a hydrogen bond to the ferryl oxygen (*17*). The structure of the HRP−acetate complex suggests that if a second hydrogen peroxide would bind to compound I in a manner similar to that in which acetate binds in the ferric enzyme, then the binding of this H_2O_2 molecule would interfere with this water (and its neighbors) in line with predictions (*51*).

High-Spin Ligand Binding to Peroxidase: Structural and Functional Implications. The EPR and UV−visible spectra of peroxidase−formate and peroxidase−acetate complexes indicate that although the iron atom may be close to hexacoordinate in the formate complex it is more likely to be pentacoordinate in the acetate complex. The red shift of the spectrum induced by acetate (Figure 2) suggests the absence of carboxyl group ligation and an indirect effect on the heme group. The mixture of EPR signals in free peroxidase (Figure 3) may reflect a mixture of hexa- and pentacoordination; addition of formate creates a single species with less rhombicity, while acetate forms a species with more pronounced rhombicity. These differences may reasonably be associated with the different iron−ligand distances and with the different orientations of the two carboxylate groups in the heme pocket (Figure 4).

High-resolution crystal structures have been reported for compounds I and II in HRP (*17*). The binding of acetate in Figures 4A suggests that a direct interaction is possible between a carboxyl group at this position and the ferryl oxygen in compound I or II as may also be possible for the corresponding orientation of the formate−catalase complex (*19*), yet although both catalase peroxide compounds react with formate (*20*, *24*, *25*) and formate is oxidized by catalase, no significant conversion of formate to carbonate has been observed in HRP under assay conditions in dilute solution (*52*). Two-electron oxidations by peroxidase seem to be confined to special pathways often involving direct oxygen atom transfer, as in sulfite oxidation (*53*) and thioanisole oxidation (*54*).

However, studies on the behavior of HRP compounds I and II in the presence of formate (P. Nicholls, unpublished results) indicate that formate may be able to interact with the peroxide compounds as well as with the free ferric enzyme. The interaction may be a catalytic one similar to that seen with catalase and involve an activation of endogenous one-electron reductant systems, but other experiments will be needed to resolve this question. Nevertheless, we believe that data presented in this paper show clearly that there are at least two stable binding orientations for the carboxylic acids in the peroxidase heme pocket, and that these structural alternatives are correlated with both the UV−visible and EPR spectroscopy of the complexes.

ACKNOWLEDGMENT

We are grateful to Andrew T. Smith (University of Sussex) for supplying purified HRP used in crystallography. The structural studies reported here were part of a project supported within a joint educational program in molecular biophysics between Uppsala University and MaxLab. We thank our students and the staff of MaxLab for their work in this project.

REFERENCES

1. Keilin, D., and Hartree, E. F. (1951) Purification of horseradish peroxidase and comparison of its properties with those of catalase and methaemoglobin, *Biochem. J. 49*, 88−104.
2. Nakajima, R., and Yamazaki, I. (1987) The mechanism of oxyperoxidase formation from ferryl peroxidase and hydrogen peroxide, *J. Biol. Chem. 262*, 2576−2581.
3. Acosta, M., Arnao, M. B., Hernandez-Ruiz, J., and Garcia-Canovas, F. (1993) Inactivation of peroxidase by hydroperoxides, in *Plant Peroxidases: Biochemistry and Physiology* (Welinder, K. G., Rassmussen, S. K., Penel, C., and Greppin, H., Eds.) pp 201−205, University of Geneva, Geneva.
4. Hernandez-Ruiz, J., Arnao, M. B., Hiner, A. N. P., Garcia-Canovas, F., and Acosta, M. (2001) Catalase-like activity of horseradish peroxidase: Relationship to enzyme inactivation by H_2O_2, *Biochem. J. 354*, 107−114.
5. Dunford, H. B. (1991) Horseradish peroxidase: Structure and kinetic properties, in *Peroxidases in Chemistry and Biology* (Everse, J., Everse, K. E., and Grisham, M. B., Eds.) Vol. 2, pp 1−24, CRC Press, Boca Raton, FL.
6. Veitch, N. C., and Smith, A. T. (2001) Horseradish peroxidase, *Adv. Inorg. Chem. 51*, 107−162.
7. Saunders, B. C., Holmes-Siedle, A. G., and Stark, B. P. (1964) *Peroxidase*, Butterworths, London.
8. Theorell, H., and Ehrenberg, A. (1952) Magnetic properties of some peroxide compounds of myoglobin, peroxidase and catalase, *Arch. Biochem. Biophys. 41*, 442−462.
9. Blumberg, W. E., Peisach, J., Wittenberg, B. A., and Wittenberg, J. B. (1968) The electronic structure of protoheme proteins. I. An electron paramagnetic resonance and optical study of horseradish peroxidase and its derivatives, *J. Biol. Chem. 243*, 1854−1862.
10. Schonbaum, G. R. (1973) New Complexes of Peroxidases with Hydroxamic Acids, Hydrazides, and Amides, *J. Biol. Chem. 248*, 502−511.
11. Schultz, C. E., Rutter, R., Debrunner, P. G., and Hager, L. P. (1984) Mössbauer and electron paramagnetic resonance studies of horseradish peroxidase and its catalytic intermediates, *Biochemistry 23*, 4743−4754.
12. Ellis, W. D., and Dunford, H. B. (1968) The kinetics of cyanide and fluoride binding by ferric horseradish peroxidase, *Biochemistry 7*, 2054−2062.
13. Job, D., and Ricard, J. (1975) Kinetic and equilibrium studies of cyanide and fluoride binding to turnip peroxidases, *Arch. Biochem. Biophys. 170*, 427−437.
14. Meunier, B., Rodriguez-Lopez, J. N., Smith, A. T., Thorneley, R. N. F., and Rich, P. R. (1998) Redox- and anion-linked protonation sites in horseradish peroxidase: Analysis of distal haem pocket mutants, *Biochem. J. 330*, 303−309.

15. Araiso, T., and Dunford, H. B. (1980) Horseradish peroxidase XLI. Complex formation with nitrate and its effect upon compound I formation, *Biochem. Biophys. Res. Commun. 94*, 1177−1182.
16. Araiso, T., and Dunford, H. B. (1981) Horseradish peroxidase. Complex formation with anions and hydrocyanic acid, *J. Biol. Chem. 256*, 10099−10104.
17. Berglund, G. I., Carlsson, G. H., Smith, A. T., Szöke, H., Henriksen, A., and Hajdu, J. (2002) The catalytic pathway of horseradish peroxidase at high resolution, *Nature 417*, 463−468.
18. Andreoletti, P., Pernoud, A., Sainz, G., Gouet, P., and Jouve, H. M. (2003) Structural studies of *Proteus mirabilis* catalase in its ground state, oxidized state and in complex with formic acid, *Acta Crystallogr. D59*, 2163−2168.
19. Loewen, P. C., Carpena, X., Rovira, C., Ivancich, A., Perez-Luque, R., Haas, R., Odenbreit, S., Nicholls, P., and Fita, I. (2004) Structure of *Helicobacter pylori* catalase, with and without formic acid bound, at 1.6 Å resolution, *Biochemistry 43*, 3089−3103.
20. Chance, B. (1950) On the reaction of catalase peroxides with acceptors, *J. Biol. Chem. 182*, 649−658.
21. Chance, B. (1952) Effect of pH on the reaction kinetics of the enzyme−substrate compounds of catalase, *J. Biol. Chem. 194*, 471−481.
22. Chance, B., and Herbert, D. (1952) The enzyme−substrate compounds of bacterial catalase and peroxides, *Biochem. J. 46*, 402−414.
23. Aebi, H., and Frei, E. (1958) Gekoppelte oxydation von formiat und thiolverbindungen durch katalase, *Helv. Chim. Acta 41*, 361−371.
24. Nicholls, P. (1961) The action of anions on catalase peroxide compounds, *Biochem. J. 81*, 365−374.
25. Maj, M., Loewen, P., and Nicholls, P. (1998) *E. coli* HPII catalase interaction with high spin ligands: Formate and fluoride as active site probes, *Biochim. Biophys. Acta 1384*, 209−222.
26. Wittenberg, J. B., Noble, R. W., Wittenberg, B. A., Antonini, E., Brunori, M., and Wyman, J. (1967) Studies on the equilibria and kinetics of the reactions of peroxidase with ligands. II. The reaction of ferroperoxidase with oxygen, *J. Biol. Chem. 242*, 626−634.
27. Willick, G. E., Schonbaum, G. R., and Kay, C. M. (1969) Circular dichroism and absorption spectra of horseradish peroxidase and sperm whale myoglobin in the Soret region, *Biochemistry 8*, 3729−3734.
28. Wittenberg, B. A., Antonini, E., Brunori, M., Noble, R. W., Wittenberg, J. B., and Wyman, J. (1967) Studies on the equilibria and kinetics of the reactions of peroxidases with ligands. III. The dissociation of carbon monoxide from carbon monoxide ferro-horseradish peroxidase, *Biochemistry 6*, 1970−1974.
29. Hayashi, Y., Yamada, H., and Yamazaki, I. (1976) Heme-linked proton dissociation of carbon monoxide complexes of myoglobin and peroxidase, *Biochim. Biophys. Acta 427*, 608−616.
30. Smith, A. T., Santama, N., Dacey, S., Edwards, M., Bray, R. C., Thorneley, R. N. F., and Burke, J. F. (1990) Expression of a synthetic gene for horseradish peroxidase C in *Escherichia coli* and folding and activation of the recombinant enzyme with Ca^{2+} and heme, *J. Biol. Chem. 265*, 13335−13343.
31. Henriksen, A., Smith, A. T., and Gajhede, M. (1999) The structures of the horseradish peroxidase C-ferulic acid complex and the ternary complex with cyanide suggest how peroxidases oxidize small phenolic substrates, *J. Biol. Chem. 274*, 35005−35011.
32. Hadfield, A. T., and Hajdu, J. (1993) A fast and portable micro-spectrophotometer for time-resolved X-ray diffraction experiments, *J. Appl. Crystallogr. 26*, 839−842.
33. Otwinowski, Z. (1993) Oscillation data reduction program, in *Data Collection and Processing* (Sawyer, L., Isaacs, N. W., and Bailey, S., Eds.) pp 55−62, SERC Daresbury Laboratory, Warrington, U.K.
34. Collaborative Computational Project, Number 4 (1994) The CCP4 suite: Programs for protein crystallography, *Acta Crystallogr. D50*, 760−763.
35. Brünger, A. T., Adams, P., Clore, G., Delano, W., Gros, P., Grosse-Kunstleve, R., Jiang, J.-S., Kuszewski, J., Nilges, N., Pannu, N., Read, R., Rice, L., Simonson, T., and Warren, G. (1998) Crystallography and NMR system (CNS): A new software system for macromolecular structure determination, *Acta Crystallogr. D53*, 905−921.
36. Lamzin, V. S., and Wilson, K. S. (1993) Automated refinement of protein models, *Acta Crystallogr. D49*, 129−149.
37. Pignol, D., Gaboriaud, C., Fontecilla-Camps, J. C., Lamzin, V. S., and Wilson, K. S. (1996) How to escape from model bias with a high-resolution native data set: Structure determination of the PcpA-S6 subunit III, *Acta Crystallogr. D52*, 345−355.
38. Lamzin, V. S., and Wilson, K. S. (1997) Automated refinement for protein crystallography, *Methods Enzymol. 277*, 269−305.
39. Perrakis, A., Sixma, T. K., Wilson, K. S., and Lamzin, V. S. (1997) wARP: Improvement and extension of crystallographic phases by weighted averaging of multiple refined dummy atomic models, *Acta Crystallogr. D53*, 448−455.
40. Rodriguez-Lopez, J. N., Smith, A. T., and Thorneley, R. N. F. (1996) Role of arginine 38 in horseradish peroxidase, *J. Biol. Chem. 271*, 4023−4030.
41. Ozaki, S., Inada, Y., and Watanabe, Y. (1998) Characterization of Polyethylene Glycolated Horseradish Peroxidase in Organic Solvents: Generation and Stabilization of Transient Catalytic Intermediates at Low Temperature, *J. Am. Chem. Soc. 120*, 8020−8025.
42. Baek, H. K., and van Wart, H. E. (1989) Elementary steps in the formation of horseradish peroxidase compound I: Direct observation of compound 0, a new intermediate with a hyperporphyrin spectrum, *Biochemistry 28*, 5714−5719.
43. Baek, H. K., and van Wart, H. E. (1992) Elementary steps in the reaction of horseradish peroxidase with several peroxides: Kinetics and thermodynamics of formation of compound 0 and compound I, *J. Am. Chem. Soc. 114*, 718−725.
44. Denisov, I. G., Markis, T. M., and Sligar, S. G. (2002) Formation and decay of hydroperoxo-ferric heme complex in horseradish peroxidase studied by cryoradiolysis, *J. Biol. Chem. 277*, 42706−42710.
45. Rodriguez-Lopez, J. N., Lowe, D. J., Hernandez-Ruiz, J., Hiner, A. N. P., Garcia-Canovas, F., and Thorneley, R. N. F. (2001) Mechanism of reaction of hydrogen peroxide with horseradish peroxidase: Identification of intermediates in the catalytic cycle, *J. Am. Chem. Soc. 123*, 11838−11847.
46. Evangelista-Kirkup, R., Smulevich, G., and Spiro, T. G. (1986) Alternative carbon monoxide binding modes for horseradish peroxidase studied by resonance Raman spectroscopy, *Biochemistry 25*, 4420−4425.
47. Barlow, C. H., Ohlsson, P.-I., and Paul, K.-G. (1976) Infrared spectroscopic studies of carbonyl horseradish peroxidases, *Biochemistry 15*, 2225−2229.
48. Feis, A., Rodriguez-Lopez, J. N., Thorneley, R. N., and Smulevich, G. (1998) The distal cavity structure of carbonyl horseradish peroxidase as probed by the resonance Raman spectra of His 42 Leu and Arg 38 Leu mutants, *Biochemistry 37*, 13575−13581.
49. Meunier, B., Rodriguez-Lopez, J. N., Smith, A. T., Thorneley, R. N., and Rich, P. R. (1995) Laser photolysis behavior of ferrous horseradish peroxidase with carbon monoxide and cyanide: Effects of mutations in the distal heme pocket, *Biochemistry 34*, 14687−14692.
50. Jarnagin, R. C., and Wang, J. H. (1958) Investigation of the catalytic mechanism of catalase and other ferric compounds with doubly O^{18}-labeled hydrogen peroxide, *J. Am. Chem. Soc. 80*, 786−787.
51. Jones, P. (2001) Roles of water in heme peroxidase and catalase mechanisms, *J. Biol. Chem. 276*, 13791−13796.
52. Keilin, D., and Hartree, E. F. (1955) Catalase, peroxidase and metmyoglobin as catalysts of coupled peroxidatic reactions, *Biochem. J. 60*, 310−325.
53. Araiso, T., Miyoshi, K., and Yamazaki, I. (1976) Mechanisms of electron transfer from sulfite to horseradish peroxidase-hydroperoxide compounds, *Biochemistry 15*, 3059−3063.
54. Harris, R. Z., Newmyer, S. L., and Ortiz de Montellano, P. R. (1993) Horseradish peroxidase-catalyzed two-electron oxidations: Oxidation of iodide, thioanisoles, and phenols at distinct sites, *J. Biol. Chem. 268*, 1637−1645.
55. Read, R. J. (1986) Improved Fourier coefficients for maps using phases from partial structures with errors, *Acta Crystallogr. A42*, 140−149.
56. Kraulis, P. J. (1991) Molscript: A program to produce both detailed and schematic plots of protein structures, *J. Appl. Crystallogr. 24*, 946−950.
57. Merritt, E., and Murphy, M. E. P. (1994) Raster3d version 2.0: A program for photorealistic molecular graphics, *Acta Crystallogr. D50*, 869−873.

58. Esnouf, R. M. (1997) An extensively modified version of MolScript that includes greatly enhanced coloring capabilities, *J Mol. Graphics Modell. 15*, 132−134.
59. Esnouf, R. M. (1999) Further additions to MolScript version 1.4, including reading and contouring of electron-density maps, *Acta Crystallogr. D55*, 938−940.
60. Brünger, A. T. (1992) The free *R* value: A novel statistical quantity for assessing the accuracy of crystal structures, *Nature 355*, 472.
61. Shimizu, H., Park, S. Y., Shiro, Y., and Adachi, S. (2002) X-ray structure of nitric oxide reductase (cytochrome P450nor) at atomic resolution, *Acta Crystallogr. D58*, 81−89.
62. Vojtechovsky, J., Berendzen, J., Chu, K., Schlichting, I., and Sweet, R. M. (1999) Implications for the Mechanism of Ligand Discrimination and Identification of Substates Derived from Crystal Structures of Myoglobin−Ligand Complexes at Atomic Resolution, *Biophys. J. 77*, 2153−2174.
63. Kachalova, G. S., Popov, A. N., and Bartunik, H. D. (1999) A steric mechanism for inhibition of CO binding to heme proteins, *Science 284*, 473−476.
64. Chu, K., Vojtchovsky, J., McMahon, B. H., Sweet, R. M., Berendzen, J., and Schlichting, I. (2000) Structure of a ligand-binding intermediate in wild-type carbonmonoxy myoglobin, *Nature 403*, 921−923.
65. Adachi, S., Park, S. Y., Tame, J. R. H., Shiro, Y., and Shibayama, N. (2003) Direct observation of photolysis-induced tertiary structural changes in hemoglobin, *Proc. Natl. Acad. Sci. U.S.A. 100*, 7039−7044.
66. Sjögren, T., Svensson-Ek, M., Hajdu, J., and Brzezinski, P. (2000) Proton-coupled structural changes upon binding of carbon monoxide to cytochrome cd_1: A combined flash photolysis and X-ray crystallography study, *Biochemistry 39*, 10967−10974.

BI0483211